Toward a Unified Scheme for the Aggregation of Tau into Alzheimer Paired Helical Filaments†

S. Barghorn and E. Mandelkow*

Max-Planck-Unit for Structural Molecular Biology, Notkestrasse 85, 22607 Hamburg, Germany

Received July 17, 2002; Revised Manuscript Received September 26, 2002

ABSTRACT: Alzheimer's disease is characterized by aggregates of tau protein. Attempts to study the conditions for aggregation in vitro have led to different experimental systems, some of which appear mutually exclusive (e.g., oxidative vs reductive conditions, induction by polyanions vs fatty acids). We show here that different approaches and pathways can be viewed in a common framework, and that apparent differences can be explained by variations in the kinetics of subreactions. A unified view of PHF aggregation should help to analyze the causes of PHF aggregation and devise methods to prevent it.

Tau is a microtubule-associated protein that occurs mainly in neurons and is involved in neurite extension and maintenance. In the human CNS, it exists as six alternatively spliced isoforms, coded on a single gene on chromosome 17, that are developmentally regulated. Tau is a highly soluble protein, its sequence is dominated by hydrophilic residues, and it has a "natively unfolded" structure in solution, consistent with its resistance to heat and acid treatment. Despite these properties, tau generates insoluble aggregates in Alzheimer's disease and related "tauopathies" which characterize degenerating neurons and correlate with the clinical stages of the dementia. The aggregates take the form of paired helical filaments (PHFs)[1] or straight filaments which associate into the higher order structures of neurofibrillary tangles (NFTs) (for overviews, see refs *1*−*4*).

Since tau aggregates are implicated in neurodegeneration it is of obvious interest to reconstitute the assembly process in vitro, in the hope of understanding the underlying principles of aggregation and discovering methods to prevent or reverse the process. Progress has been slow because of two major issues: Due to its hydrophilic nature, recombinant tau (or tau isolated from brain tissue) shows very little intrinsic tendency to aggregate, making it difficult to follow the stages of aggregation by biochemical or spectroscopic methods. Furthermore, the structure of tau aggregates is ill-defined on a molecular level, leaving uncertainties on whether the aggregates obtained in vitro are equivalent to those of Alzheimer's disease. During the past decade, the problems of slow aggregation rate and low yield have been alleviated by a combination of several advances: (a) choice of suitable tau domains, e.g., the repeat domain alone aggregates more readily into bona fide PHFs than full-length tau (*5*−*7*), (b) addition of cofactors which increase reaction rates, such as polyanions (e.g., heparin, poly-Glu, RNA (*8*−*10*)) or fatty acids (e.g., arachidonic acid (*11*, *12*)). In addition, methods have been worked out that yield reliable estimates of aggregation in solution and in real time, such as the fluorescence of added reporter dyes (thioflavine S) or light scattering (*7*, *13*). These methods have allowed better insights into factors that play a role in tau's pathological aggregation. For example, it can be described as a nucleation−elongation reaction (*14*), it involves the formation of beta-structure around some hexapeptide motifs in the repeat domain (*15*−*17*), and the repeat domain forms the core of tau fibers reconstituted from recombinant tau, similar to the fibers from Alzheimer brain (*18*−*20*). Apart from this, little progress has been made in understanding the packing of tau in the fibers, mainly because high resolution structures of tau or tau aggregates are not available so far. The judgment on realistic assembly conditions still relies on electron microscopy which shows whether fibers are "paired helical" or not, because this feature, with its typical 80 nm crossover repeat, is characteristic of Alzheimer PHFs. Straight filaments can be formed as well, but in this case the discrimination from other types and pathways of aggregation is less clear-cut. These issues are of practical importance since there is a need for developing reliable aggregation assays that allow the testing of inhibitory substances and lend themselves to high throughput format.

Currently, the two best-studied aggregation assays make use of the addition of either polyanions or fatty acids, and they are performed in oxidative or reductive conditions, respectively (other buffer conditions being comparable, i.e., pH around 7, ionic strength around 100 mM, room temperature to 37 °C). Since the resulting structures tend to differ as well (predominantly paired helical vs straight fibers), one may ask whether there is a principal difference between these aggregation pathways and products that may result from different types of subunit packing. This was the question addressed in this study. We conclude that the differences and seeming contradictions in reported assembly conditions are not fundamental. They concern mainly differences in

† This work was supported in part by the Deutsche Forschungsgemeinschaft.

* Corresponding author: Tel: +49−40−89982810. Fax: +49−40−89716822. E-mail: mand@mpasmb.desy.de.

[1] Abbreviations: AA, arachidonic acid; CMC, critical micelle concentration; DTT, dithiothreitol; FTDP-17, frontotemporal dementia and parkinsonism linked to chromosome 17; PBS, phosphate buffered saline; PHF, paired helical filaments; PMSF, phenylmethylsulfonyl-fluoride; ThS, thioflavine S.

10.1021/bi026469j CCC: $22.00
Published on Web 11/20/2002

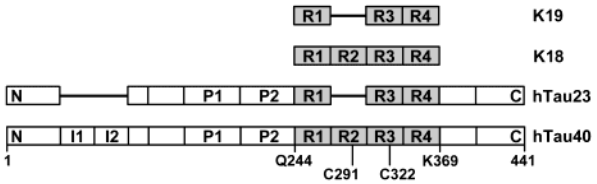

FIGURE 1: Diagram of tau isoforms and tau derived constructs.The lower bar shows htau40, the largest isoform in the human CNS (441 residues). The C-terminal half contains three or four pseudo-repeats (~31 residues each, R1−R4, gray shade) which together with their proline-rich flanking regions constitute the microtubule-binding domain. Repeat R2 and the two near N-terminal inserts (I1, I2) may be absent due to alternative splicing, as in htau23, the shortest human isoform. Construct K18 comprises only the four repeats (residues Q244-E372; 129 residues), construct K19 (98 residues) comprises only three repeats. The two cysteines of tau are located in the third repeat (C322 in R3) and the second repeat (C291 in R2) which is absent in three-repeat isoforms. In the mutants, one or both of the cysteines were replaced by alanine or glycine (see text). In oxidizing conditions, tau with one cysteine can form a covalent dimer which promotes PHF aggregation. Two cysteines allow either a covalent dimer or a "compact monomer" containing an intramolecular disulfide bridge between C291 and C322.

kinetic parameters, i.e., rates of dimerization, nucleation, elongation, or inhibition by unproductive side reaction, but the basic interactions between aggregation of tau molecules appear to be comparable. Thus, the different experimental approaches can be summarized in a common overall reaction scheme.

MATERIALS AND METHODS

Chemicals and Proteins. Thioflavine S, arachidonic acid, and heparin (average MW of 6000) were obtained from Sigma (Steinheim, Germany). The human tau isoforms (htau40, htau23) and tau constructs (K18, K19) (see Figure 1) were expressed in *Escherichia coli* as described (*21*). The numbering of the amino acids is that of the isoform htau40 containing 441 residues (*22*). The protein was expressed and purified as described elsewhere (*23*) making use of the heat stability and FPLC Mono S chromatography with subsequent gel-filtration (Superdex 200 for tau isoforms (htau40, htau23) and Superdex 75 for tau constructs (K18, K19) (Amersham Pharmacia Biotech, Freiburg, Germany). The purity of the proteins was analyzed by SDS−PAGE. Protein concentrations were determined by the Bradford assay or by UV-absorption at 214 nm against a BSA standard curve. The tau mutations were created by site-directed mutagenesis which was performed using the QuikChange site-directed mutagenesis kit (Stratagene, Amsterdam, Netherlands) and the plasmid pNG2 (*23*). Plasmids were sequenced on both strands.

PHF Assembly. Aggregation was induced by incubating varying concentrations of tau isoforms or tau constructs (typically in the range of 4−50 μM) in volumes of 20−500 μL at 37 °C in PBS pH 7.4 (137 mM NaCl, 3 mM KCl, 10 mM Na_2HPO_4, 2 mM KH_2PO_4, ionic strength ~160 mM) with 1 mM DTT and mixing it with the anionic cofactor heparin (MW ≈ 6000 Da, used in a molar ratio of tau/heparin of 4:1), and observed by thioflavine S fluorescence of aliquots withdrawn at different time points (*7*). Aggregation of tau with arachidonic acid (75 μM) was done as described by Binder and co-workers (*12*, *24*) but in PBS buffer pH 7.4 as above, with 1 mM DTT and mixing it with the free fatty acid arachidonic acid. Note that the solvent for the arachidonic acid is 100% ethanol and PHF-assembly samples therefore finally contained 3.75% ethanol. In some experiments, the protein was preoxidized in PBS buffer without DTT and without heparin or arachidonic acid to allow enhanced disulfide formation by air oxidation. Incubation times for filament formation varied from minutes up to several days. In the case of incubation times that exceeded 2 days tau solutions (only valid for tau isoforms and not tau constructs) were supplemented with a protease inhibitor mix containing 1 mM PMSF, 1 mM EDTA, 1 mM EGTA, 1 μg/mL leupeptin, 1 μg/mL aprotinin, and 1 μg/mL pepstatin. The formation of PHFs was monitored by thioflavine S fluorescence (which increases upon tau aggregation), electron microscopy (which allows visualization of filaments and their twisted appearance), and FTIR spectroscopy (which distinguishes between random coil and beta sheet structures) (*7*, *15*, *16*, *25*).

Fluorescence Spectroscopy. Aggregation was monitored by fluorescence of thioflavine S using a Fluoroskan Ascent spectrofluorimeter (Labsytems, Helsinki, Finland) with an excitation filter of 440 nm and an emission filter of 510 nm in a 384 well plate. Measurements were carried out at room temperature in PBS pH 7.4 with 10 μM ThS unless otherwise stated. Background fluorescence and light scattering of the sample without ThS was subtracted when needed. Measurements were typically done in triplicate, the curves show the average values and standard deviations represented by the error bars (note that in some cases the bars are not visible because they lie within the symbols).

Electron Microscopy. For ascertaining the formation of PHFs, 10 μL protein solutions diluted to 1−10 μM protein were placed on 600-mesh carbon-coated copper grids for 45 s, washed twice with H_2O and negatively stained with 2% uranyl acetate for 45 s. The specimens were examined with a Philips CM12 electron microscope at 100 kV.

Blue Native Polyacrylamide Gel Electrophoresis. BN−PAGE was performed as described (*26*). In brief, a polyacrylamide gradient from 5 to 18% in 50 mM Tris, 34 mM HCl, 5% glycerol (pH 8.5 at 4 °C) was used. The acrylamide solution contained one part 40% acrylamide/bis-acrylamide (38:2) und four parts 40% acrylamide/bis-acrylamide (37.5:1). The stacking gel had a concentration of 5% acrylamide in the same buffer as the separation gel. Electrophoresis was carried out in a cathode buffer containing 25 mM Tris, 20 mM tricine, and 0.02% Coomassie brilliant blue G-250 (AppliChem) (w/v) (pH 8.5 at 4 °C) and an anode buffer of 50 mM Tris, 34 mM HCl (pH 8.5 at 4 °C). The protein bands, which were already Coomassie stained during the electrophoresis, were quantified using the TINA-software version 2.01 (Raytest, Straubenhardt, Germany). For better visualization, gels were destained subsequently and silver stained (modified after Heukeshoven and Dernick, 1988 (*27*)).

RESULTS

(a) Role of Disulfide Cross-Links in Tau Aggregation. Tau is an unusually soluble protein and shows practically no tendency to aggregate in normal buffer conditions, due to its hydrophilic nature (*28*, *29*). Thus, its aggregation in

diseased neurons is counterintuitive. Our earlier attempts to accelerate tau's aggregation in vitro had revealed several important factors: (a) Shorter tau constructs comprising the repeat domain aggregated faster than full-length isoforms (*5*−*7*), (b) oxidizing conditions generated disulfide-linked dimers which appeared to serve as building blocks (*5*, *6*). (c) In addition, polyanions greatly improve polymerizability (*8*−*10*). (d) The nucleation barrier, the rate-limiting step in PHF formation, can be overcome by adding to a tau solution small amounts of PHFs isolated from Alzheimer brains or generated in vitro which act as seeds for polymerization (*14*). (e) Certain hexapeptide motifs in the second ($_{275}$VQIINK$_{280}$) or the third repeat ($_{306}$VQIVYK$_{311}$) are critical for PHF-assembly by forming a β-sheet structure upon PHF polymerization. Some FTDP-17 mutations lying within or close to these hexapeptides, such as ΔK280 or P301L, accelerate PHF aggregation by enhancing β-sheet propensity (*16*, *25*). On the basis of these factors, we developed a real-time assembly assay based on the fluorescence of thioflavine S which allowed kinetic studies and revealed distinct stages of aggregation (*7*, *14*). On the other hand, Binder and coworkers developed aggregation conditions that were formally different, requiring free fatty acids (e.g., arachidonic acid) and reducing conditions (*11*, *12*). One possibility to explain the differences would be that different polymorphic aggregates might be formed in the two cases; alternatively, it is possible that the aggregates are similar, and only the stages and kinetics of the assembly pathway might be different. These issues are important when one is seeking factors and conditions to prevent or slow the pathological aggregation of tau.

To investigate this, we generated new constructs and mutants of tau that affect the kinetics of aggregation and studied their assembly behavior and structures. There are six isoforms of tau in human CNS; we expressed the shortest and the longest (htau23 and htau40), as well as their repeat domains (K19 and K18, Figure 1) because they represent the core of the microtubule-binding domain as well as the core of Alzheimer-PHFs (*18*, *19*). Due to alternative splicing of exon 10, the repeat domains differ by one repeat, R2 (note that different conventions for defining the repeats are in use; in our terminology R2 comprises 31 residues and is coded by exon 10). Tau contains two cysteines, C291 and C322. C322 is present in all isoforms, but C291 is present only in four-repeat isoforms because it lies in R2. Since these residues are involved in disulfide cross-linking and aggregation, we mutated them into neutral residues (Ala or Gly), either singly or in combination. We also created constructs in combination with ΔK280 mutants, lacking K280 which is one of the mutations found in FTDP-17 (*30*). This mutant has the unique property of readily aggregating into PHFs even without polyanions (*16*, *25*).

Figure 2A illustrates the aggregation of K19 (repeat domain with three repeats), induced in the presence of polyanions (heparin) with or without reducing agent (DTT). Aggregation typically takes place over 2−3 days, whereas the protective effect of 1 mM DTT during air oxidation lasts only 20−25 h (half time ∼9 h in these conditions, data not shown). As expected, DTT reduces both the rate and extent of aggregation (Figure 2A, lower curve). This is consistent with the earlier observation that dimers cross-linked at C322 are important in facilitating aggregation (*5*, *6*). By contrast,

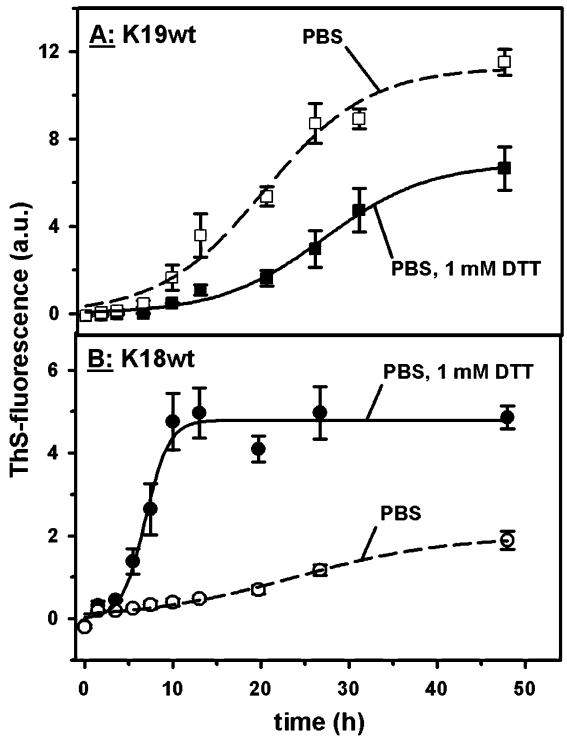

FIGURE 2: Aggregation of the repeat domain (constructs K18, K19) into paired helical filaments in reducing and oxidizing conditions. The kinetics of aggregation was measured fluorimetrically using the thioflavine S assay (*7*). Tau protein concentrations were 20 μM, heparin 5 μM in PBS pH 7.4 containing either 1 mM DTT (closed symbols, solid lines) or no DTT (open symbols, dashed lines). Shown is the average value ($n = 3$) with the standard deviation represented by the error bars (note that some error bars lie within the symbols). (A) In oxidizing conditions (absence of DTT) the aggregation of the three-repeat construct K19 (containing only C322 in R3) is increased in rate and extent, compared to reducing conditions (presence of DTT), because covalent dimers (by intermolecular disulfide bridges) promote aggregation. (B) By contrast, the four-repeat construct K18 (containing C322 in R3 and C291 in R2) shows reduced filament formation under oxidizing conditions because compact monomers (by intramolecular disulfide bridges) are inhibitory for aggregation.

the reverse behavior is found with the four-repeat construct K18 (Figure 2B). This seeming contradiction is explained by the fact that 4R-tau preferably forms intramolecular disulfide cross-links in oxidizing conditions (C291−C322) which have previously been identified by native PAGE and termed "compact monomers" (*6*). These compact monomers do not participate and even inhibit aggregation into PHFs because they are locked in the wrong conformation. However, when the two cysteines are kept in a reduced state, aggregation readily takes place in the presence of polyanions (Figure 2B, top curve). In either case, without polyanions aggregation is very slow and not measurable in real time with the ThS assay. From these data we conclude: (a) Polyanions generally promote tau aggregation. (b) Tau dimers, formed by disulfide cross-linking of 3R-tau, promote aggregation. (c) Intramolecular cross-linking of 4R-tau into compact monomers inhibits aggregation. However, the data also show that covalent dimerization of tau is not an absolute requirement, i.e., in the presence of polyanions one can obtain aggregates even in reducing conditions. Electron microscopy (see below) confirms that the aggregates described here have the typical appearance of paired helical or straight filaments.

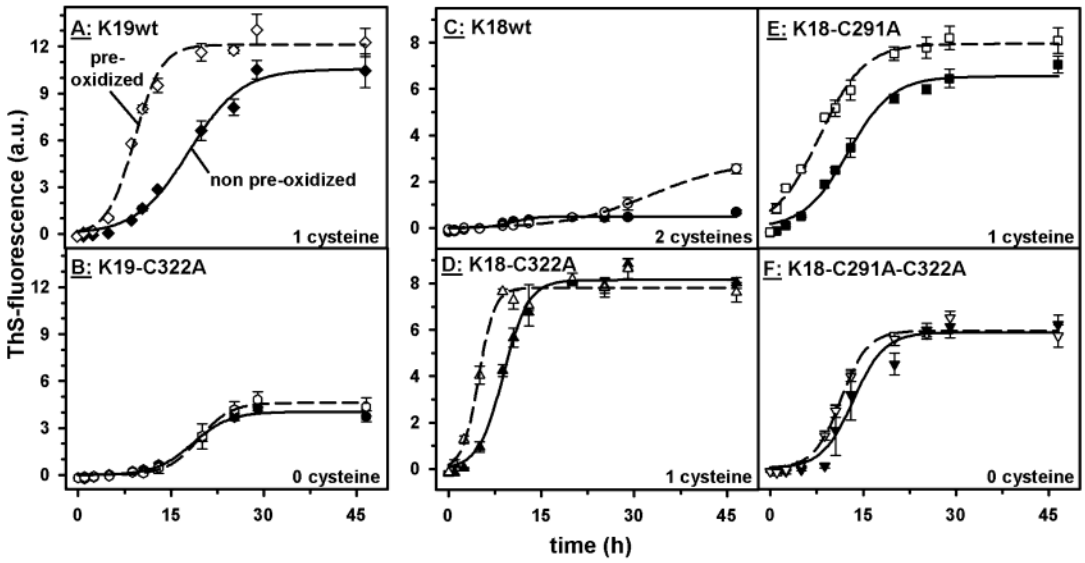

FIGURE 3: Aggregation of K18 and K19 constructs and their cysteine mutants in oxidizing conditions. The kinetics of aggregation was measured fluorimetrically using the ThS assay, using heparin as the promoting polyanion. Tau protein concentrations were 10 μM, heparin 2.5 μM in PBS pH 7.4. Shown is the average value ($n = 3$) with the standard deviation. Before adding heparin and measuring aggregation kinetics, half of the protein was preincubated (without DTT) for 3 days at 37 °C to increase the fraction of dimers (open symbols, dashed lines), the other half was used immediately upon unfreezing (closed symbols, solid lines). Both protein samples were then mixed with heparin and used for the aggregation assay. Note that both samples were stored without DTT. (A, D, E) Construct K19 (A) forms aggregates (solid line), preincubation accelerates aggregates because of disulfide-cross-linked dimers (dashed lines). The same behavior is observed for K18 mutants carrying only one cysteine, K18-C322A (D) and K18-C291A (E). (B, F) Aggregation of tau occurs even in the complete absence of cysteines, as in the case of K19-C322A (B) or K18-C291A-C322A (F), but there is no additional gain by preincubation since no disulfide cross-links can be formed. (C) K18 containing two cysteines shows almost no aggregation, due to the inhibitory effect of intramolecular disulfide bridges in oxidizing conditions.

As a next step, we checked the above interpretations using tau constructs that lack one or both cysteines. Aggregation was induced by heparin in oxidizing conditions (without DTT), and aliquots were preincubated for 3 days in buffer without heparin to allow disulfide cross-linking. As an example, the 3R-construct K19 aggregates as expected (half time ~17 h), but preoxidation further accelerates aggregation once heparin is added (half time ~6 h) due to the increase in dimers cross-linked at C322 (Figure 3A). An analogous behavior can be seen with the 4R-construct K18 where one of the cysteines is eliminated, such as K18-C322A or K18-C291A (Figure 3D,E). When no disulfide cross-links can be formed, aggregation still occurs, but preincubation has no further effect (as in K19-C322A, or in the double mutant K18-C291A-C322A, Figure 3B,F). Finally, when two cysteines are present, as in K18, oxidation leads mostly to "compact monomers" which inhibit aggregation (Figure 3C) (*6*, *31*). In the absense of polyanions, these observations have an all-or-none character within the experimental time frame, but with polyanions they are now transformed into relative rates (faster or slower). That is, disulfide cross-links which generate tau dimers enhance aggregation, but aggregation is possible even without covalent dimers, presumably because dimers also exist in a noncovalent form.

Thus far, the experiments were conducted with the repeat domain, but since Alzheimer PHFs contain all full-length tau isoforms it was important to demonstrate their behavior. The main difference is that full-length tau aggregates much more slowly (at least in the presence of polyanions), with half times in the range of 4−8 days (Figure 4). Apart from this, the dependence on cysteines and oxidation was comparable to that of the repeat domain alone. The juvenile isoform htau23 and its cysteine-less mutant htau23-C322G aggregated slowly but with comparable speeds in the presence of heparin (Figure 4A, solid and dashed lines). By contrast, oxidation by preincubation lead to much faster aggregation of htau23 wild-type (dotted line) due to the generation of covalent dimers (~40% of the total protein). Likewise, the four-repeat isoform htau40 and its cysteine-less mutant htau40-C291A-C322G aggregated with similar rates in reducing conditions (Figure 4B). Aggregation of htau40 in oxidative conditions was much less efficient because of the inhibition by compact cross-linked monomers (data not shown). The experiments corroborate previous conclusions that dimerization by disulfide cross-linking accelerates aggregation, but they also show that dimerization is less important in the presence of assembly promoting polyanions.

To measure the aggregation of tau in solution, it is usually necessary to speed up rates by a polyanionic cofactor, and therefore the influence of the cofactor on other properties is difficult to ascertain. An exception to this rule is the mutant K18-ΔK280 because of its high propensity for beta-structure interactions (*16*). With heparin, it aggregates within hours (Figure 5A, solid curve), but even without heparin or other cofactors it aggregates in a few days (Figure 5B, solid curve). Elimination of cysteines (as in K18-ΔK280-C291A-C322A) reduces aggregation rates, especially without heparin (Figure 5A,B, dashed curves), but still allows the formation of bona fide PHFs (see below), confirming that covalent dimers accelerate the kinetics but are not essential for aggregation.

(b) Structure of Tau Aggregates and Its Cysteine Mutants Induced with Heparin: 3R-tau Forms Preferentially Twisted Fibers. The ThS assay used in the above experiments is a reliable indicator of aggregation but does not reveal the structure of the aggregates. We therefore checked them by negative stain electron microscopy (Figure 6). Most fibers

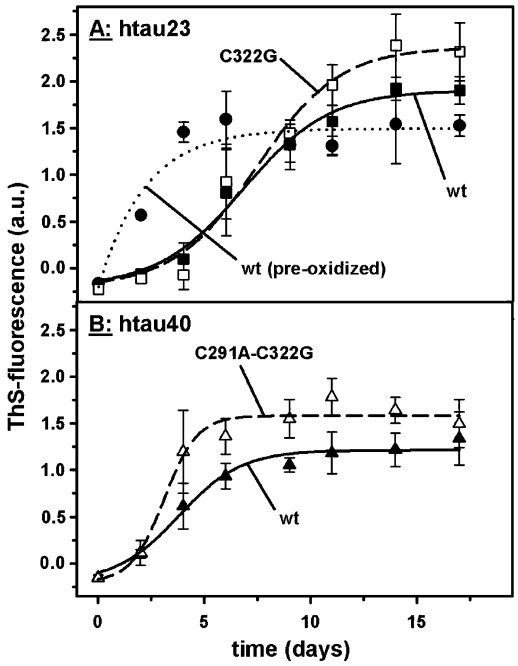

FIGURE 4: Aggregation of htau23 and htau40 and their cysteine-mutants in reducing conditions.The kinetics of aggregation of htau23 and htau40 was measured fluorimetrically using the ThS assay. Tau protein concentrations were 45 μM, heparin 11.25 μM in PBS pH 7.4, 2 mM DTT. To maintain reducing conditions over long periods 1 mM DTT was added to the samples every day. Shown is the average value ($n = 3$) with the standard deviation. (A) Aggregation of the three-repeat isoform htau23 (solid curve) and the mutant without the cysteine (htau23-C322G) aggregate with a comparable velocity and extent. Preincubation for 3 days at 37 °C without heparin or DTT favors dimerization by disulfide cross-linking and thus accelerates aggregation (dotted line). (B) Aggregation of the four-repeat isoform htau40 and its cysteine-less mutant (htau40-C291A-C322A) polymerize to filaments with a comparable velocity and extent as the wild-type.

had diameters around 9−24 nm (thin and wide regions of PHFs) or 15−17 nm (straight filaments). Typically, there was a mixture of PHFs in the strict sense (with repeats around 80 nm) and less twisted or straight filaments. For three-repeat constructs (K19 and its mutants) the twisted structures were predominant. This implies that the repeat domain follows a similar building plan as full-length tau in Alzheimer's disease, and that exchange of C322 has no influence on the structure (Figure 6A, right). Covalently cross-linked tau dimers have no recognizable effect on the appearance of the filaments. The four-repeat constructs showed a less pronounced twist and more straight fibers, particularly the C291A mutant (Figure 6A, left). The same features were present in the fibers formed from full-length tau isoforms, i.e., for htau23 (= three-repeat tau) and its mutants the PHF-like structure predominated, whereas htau40 (with four repeats) showed predominantly straight and less twisted filaments (Figure 6B). Remarkably, the diameters of fibers aggregated from the repeat domain and from full-length tau are quite similar. This implies that the repeat domain dictates the assembly properties, and that the extra mass of full-length tau (∼75% of the protein) is largely invisible by negative stain EM. This observation fits with observations that the structural core of PHFs is made up of the microtubule binding region, and that pronase digestion removes N- and C-terminal parts of tau lying outside (*18*, *19*). In addition, immunogold labeling of PHFs, using antibodies against the terminal domains, showed that the gold particles occurred some distance away from the core, not on the core itself (*32*, *33*). The low contrast is consistent with the hydrophilic nature of the protein (see ref *5*), but note that the full-length tau tended to have somewhat blurred edges which would reflect the protruding domains of the protein (Figure 6B). Finally, the four-repeat construct K18-ΔK280 and its cysteine mutants form exceptionally regular PHF structures, independently of the cysteines (Figure 6C). This argues that the extra repeat R2 (compared with K19) does not alter the building plan, and that a high propensity for beta-structure favors a pronounced twist (compare Figure 6A right and 6C).

(c) Formation of Noncovalent Dimers Occurs Independently of Cysteines. We have shown above that covalent dimerization of tau via an intermolecular disulfide bridge accelerates filament formation, but on the other hand aggregation is also possible after removal of the cysteines (Figures 3 and 4). This raises the question to what extent dimers really participate in aggregation. While tau mutants lacking cysteines cannot dimerize via a covalent disulfide bridge, dimerization via noncovalent interactions might still occur. To test this possibility, the tau constructs K18 and K19 were incubated for 3 days at 37 °C without any filament inducing substances and without DTT and then assayed by blue native polyacryamide gel electrophoresis (Figure 7). In the case of K19, this lead to ∼43% of the protein in the form of dimers, ∼56% as monomers and the rest being higher order oligomers (lane 1). Exchange of C322A strongly reduced the tendency to dimerize, emphasizing the importance of C322 for dimerization, but a clear signal of dimers remained (lane 2). Although the fraction is small (∼1%), it would suffice to accelerate the nucleation of PHFs once heparin is added. An analogous but more complex situation exists for K18. The wild-type protein shows a pronounced band of dimers (∼5%, lane 3) which could be homotypic (C291−C291 or C322−C322) or heterotypic (C291−C322). The majority of the protein is still monomeric (∼95%), compatible with the ready formation of compact monomers covalently cross-linked by C291−C322 (an intramolecular disulfide bridge previously shown by Schweers et al. 1995 (*6*)). If one of the two cysteines is replaced, the remaining single cysteine strongly enhances dimerization, as in C291A or C322A (lanes 4 and 5). However, even when both cysteines are replaced, a clear tendency for noncovalent dimers remains (∼2%, lane 6). The same picture applies to the ΔK280 mutants of K18: pronounced formation of covalent dimers when the cysteines are present (as in the wild-type protein, compare lanes 7 and 3), persistence of noncovalent dimers even when cysteines are removed (compare lanes 8 and 6). We conclude that proteins with a single cysteine have a strong tendency for dimerization, with two cysteines the formation of internal disulfide cross-links becomes dominant (and inhibitory for aggregation), but even without cysteines tau can form noncovalent dimers which would facilitate aggregation reactions.

(d) Tau Aggregation Induced by Fatty Acids Follows Similar Principles as Induction by Polyanions. The aggregation of tau by free fatty acids, in particular arachidonic acid (AA), has been explored by Binder and colleagues (*11*−*13*, *24*). Their buffer conditions were similar to ours (∼neutral pH, ∼0.1 M ionic strength, 37 °C), but emphasis was placed

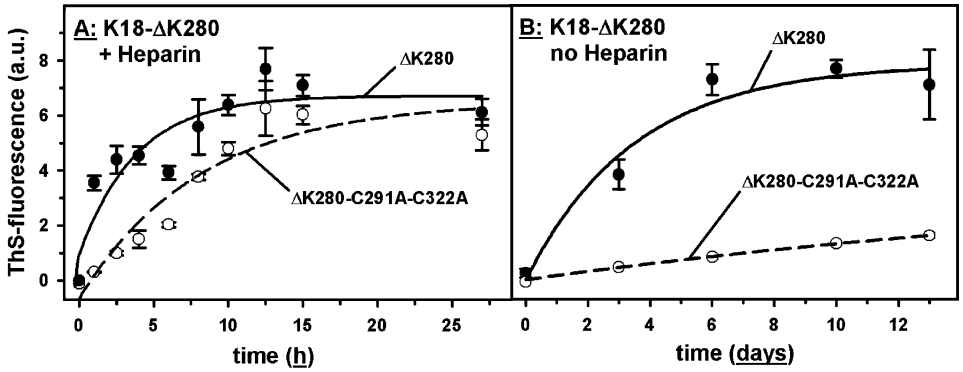

FIGURE 5: Aggregation of K18-ΔK280 construct and its cysteine-mutant into paired helical filaments under reducing conditions. The kinetics of aggregation of K18-ΔK280 into PHFs was measured fluorimetrically using the ThS assay. Shown is the average value ($n = 3$) with the standard deviation. (A) In the presence of heparin (2.5 μM; protein concentration 10 μM in PBS pH 7.4, 1 mM DTT) the mutant K18-ΔK280 aggregates with a half time of ~2 h (solid line, closed circles). The K18-ΔK280-C291A-C322A mutant with no cysteines (dashed line, open circles) shows comparable filament formation. (B) The mutant K18-ΔK280 aggregates even in the absence of heparin (protein concentration 60 μM in PBS pH 7.4, 1 mM DTT), although at a reduced rate (half time ~5 days, solid line, open circles). Even the cystein-less derivative K18-ΔK280-C291A-C322A (dashed line, open circles) still shows filament formation activity, although to a lower extent compared to K18-ΔK280 (solid line, closed circles).

on reducing conditions (in contrast to our earlier emphasis on oxidation and heparin as inducing agent (*14*, *15*)). The resulting aggregates were mainly of the "straight filament" type. Because of these differences we wanted to ascertain whether the aggregation of our tau constructs and isoforms in AA would be compatible with the same general reaction scheme as that developed above. Figure 8 shows assembly curves of the repeat domain with three and four repeats (K19, K18, Figure 8A) and corresponding full-length tau (htau23, htau40, Figure 8B) in reducing and oxidizing conditions. The induction of tau aggregates by AA shows several differences compared to that described above and in earlier studies:

(i) Upon addition of AA there is a rapid initial increase of ThS fluorescence lasting 1−5 min. This is not due to PHF formation, as almost no aggregates can be seen by EM during this phase (see below). Nevertheless, the rapid fluorescence gain reflects polymerizability of tau, because it is greatest with efficiently polymerizing tau variants, as judged by parallel electron microscopy (e.g., htau40), low with variants that polymerize poorly (e.g., htau23 or Pro-mutants), and absent with globular control proteins that show no aggregation at all (e.g., RNase, BSA, data not shown). Furthermore, the rapid phase is observed only at elevated AA concentrations, above the critical micelle concentration (CMC). We therefore ascribe this phase to formation of micelles with negative surfaces, onto which some "nucleating structure" of tau is assembled which binds ThS in a PHF-like fashion (with high fluorescence intensity). The double Pro-mutants of K18 or htau40 serve as interesting controls. Their two beta-structuring hexapeptide motifs are disrupted by the mutations I277P and I308P which inhibits proper fiber formation (*16*) but still allows some initial steps in nucleation and ThS binding (in contrast to BSA or RNase whose signals remain almost zero).

(ii) After the rapid initial phase, the ThS signal may show slow variations (increases or decreases), but these do not correlate quantitatively with the extent of aggregation, as judged by electron microscopy which reveals a gradual increase of fibers. This means that ThS fluorescence is not useful for quantitation of PHF assembly in these conditions, but conversely it suggests that most tau molecules are converted to a "high fluorescence" state (in terms of ThS reporter binding) during the early phase. By implication, the subsequent slow changes reflect redistribution, e.g., by annealing of small nonfibrous oligomers to extended fibers, without a drastic overall change in fluorescence capacity. The main exception is htau40 which shows a prolonged increase in ThS fluorescence (Figure 8B, top curves). This behavior is distinct from the aggregation of tau induced by heparin which can be monitored reliably with ThS fluorescence. It means that the generation of visible PHFs in the presence of AA cannot be quantified reliably by ThS fluorescence so that other methods are more appropriate, such as light scattering (*13*).

For the experiments described above, the buffer conditions (75 μM AA, and PBS-buffer, pH 7.4 consisting of 137 mM NaCl, 3 mM KCl, 10 mM Na_2HPO_4, 2 mM KH_2PO_4, 1 mM DTT) differ somewhat from the ones used by Binder's (75 μM AA, 10 mM HEPES, 100 mM NaCl, 5 mM DTT, pH 7.6). To rule out a specific buffer effect on PHF-formation and additional effects on AA-micelle formation (in terms of the CMC) we performed a comparative PHF-assembly study and found that the assembly kinetics nearly coincided (data not shown), confirming that these conditions lead to comparable results in terms of PHF structure and aggregation.

(iii) There is no clear distinction between oxidizing and reducing conditions, neither for 4R-tau forms (K18 or htau40, solid lines in Figure 8A,B), nor for 3R-tau forms (K19 or htau23, dashed lines in Figure 8A,B). The observed differences in ThS fluorescence are relatively small and not reliable with regard to the extent of aggregation. Our interpretation is that dimerization by cross-linking is not a major factor for aggregation, possibly because the nucleation capacity of the AA micelles is high and overrides the dimer dependence.

(iv) Conversely, the nature of the N-terminal projection domain, especially the inserts, strongly influence aggregation. The repeat domains (K18, K19) have comparable fluorescence levels after the initial rapid phase (~7−12 on the scale of Figure 8A), similar to full-length tau (Figure 8B), whereas the insert-less tau (htau23) remains at a low level and shows fewer filaments by electron microscopy. This is the opposite of heparin-induced aggregation where the N-terminal region retards aggregation (*10*). Note that in the full-length tau

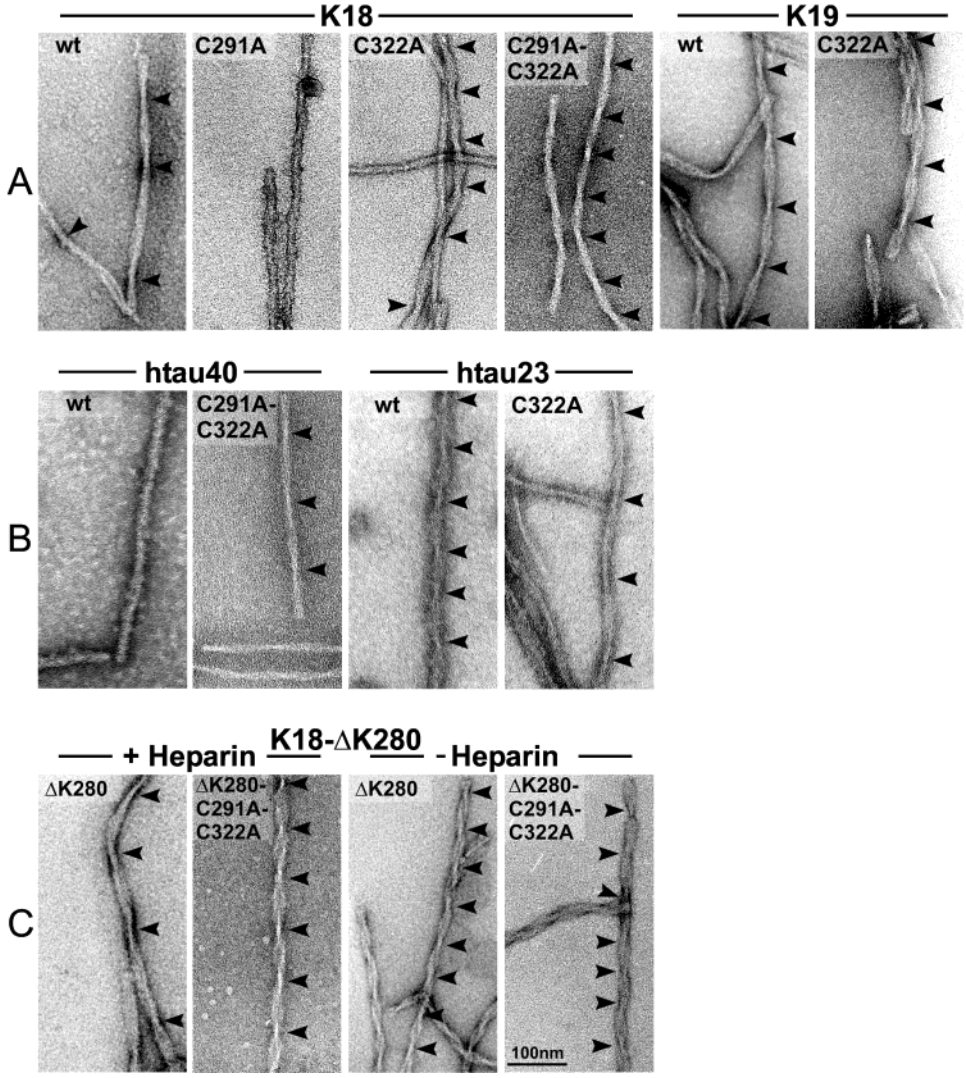

FIGURE 6: Negative stain electron microscopy of filaments of tau mutants polymerized with heparin. Filaments of tau isoforms or constructs and their cysteine mutants assembled in the presence of heparin (unless otherwise stated). Note that the same filament preparations were used as for the kinetic data (see Figures 3−5) at the endpoint of assembly). Bar in C = 100 nm. (A) The four-repeat tau constructs K18 wild-type, C322A and C291A-C322A showed filaments with the typical paired helical structure as well as straight filaments. In contrast, C291A formed predominantly straight filaments. The three-repeat tau constructs K19 wild-type and C322A showed mostly paired helical structure. (B) The four-repeat tau isoform htau40 wild-type and C291A-C322G showed mostly straight filaments. The three-repeat tau-isoform htau23 wild-type and C322G showed filaments with the typical paired helical structure as well as straight filaments. (C) The four-repeat tau constructs K18-ΔK280 and K18-ΔK280-C291A-C322A showed the typical paired helical structure independent of the polymerization in the presence or absence of heparin.

isoforms, oxidation causes a retardation in the rising phases (open circles and squares for oxidized htau40 and htau23). These findings are broadly consistent with those of Binder's group who observed little aggregation with insert-less tau and oxidative conditions (*24*). This could be explained by an assembly incompetent conformation where the C-terminal tail of tau was folded over the repeat domain (*12*, *34*, *35*). The inhibition could be relieved by the N-terminal domain with inserts (as in htau40), but not without inserts (as in htau23) (*24*).

The arachidonic acid induced aggregation products of tau were monitored in all stages with electron microscopy (Figure 9). The results confirm that the Pro-mutants of htau40 or K18 do not form filamentous aggregates, and that even htau23 shows only a low extent of aggregation, consistent with its low initial ThS signal. In oxidative conditions, 3R-tau generates mainly twisted fibers similar to PHFs (Figure 9C,F), whereas the fibers are straight in reducing conditions (Figure 9B,E). 4R-tau (K18, htau40) assembles predominantly into straight untwisted fibers, both in oxidative and reductive conditions (Figure 9A,D). This is roughly in agreement with heparin-induced aggregation where the twisted appearance dominates with 3R-tau (Figure 6 and ref *9*). It is also notable that oxidative conditions generate much shorter filaments, down to the size of "bowtie" stubs typical of broken Alzheimer PHFs, possibly because nucleation is more favored, or because they are more fragile (e.g., Figure 9F, see also ref *36*). The dimensions of the fibers (diameters, crossover periodicities) are indistinguishable within error from the fibers induced by heparin (see above). In particular, the fibers from repeat constructs have similar diameters to those from full-length tau isoforms, arguing that the extra mass outside the repeat domain is nearly invisible by negative stain electron microscopy.

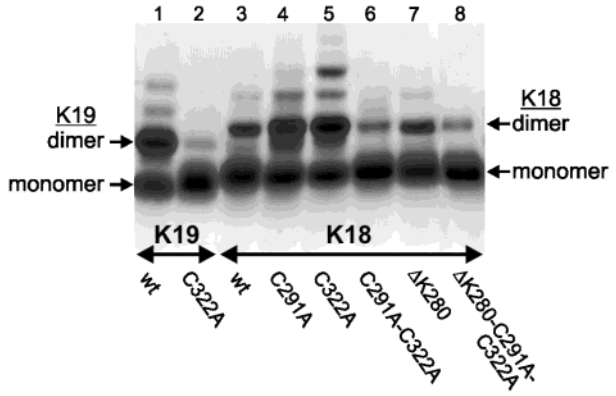

FIGURE 7: Blue native polyacrylamide gel electrophoresis of K18 and K19. A blue native polyacrylamide electrophoresis of the tau repeat constructs K18 and K19 and their cysteine mutants was performed. The gel was loaded with 0.7 μg protein after an incubation for 4 days at 37 °C in PBS pH 7.4, 1 mM DTT (the DTT will be consumed after ~1 day) to induce dimerization (protein concentration: K18 = 12 μM and K19 = 24 μM). The three-repeat tau constructs K19 and the mutants of the four-repeat construct K18 (K18-C291A and K18-C322A) contain only one cysteine and dimerize to a high extent (between 28 and 43%) due to the formation of an intermolecular disulfide bridge. Although containing no cysteins the mutants K19-C322A, K18-C291A-C322A and K18-ΔK280-C291A-C322A form to low extent (about 1−2%) dimers via noncovalent interactions. The K18wt protein contains two cysteins and forms only to a low extent dimers (5%) due to the preferential formation of intramolecular disulfides. Note that the quantitation is based on Coomassie stained protein bands. For better visualization gels were destained subsequently and silver stained as shown here (see Methods). Due to the nonquantitative nature of the silver staining procedure protein bands may not appear in their correct ratio to each other.

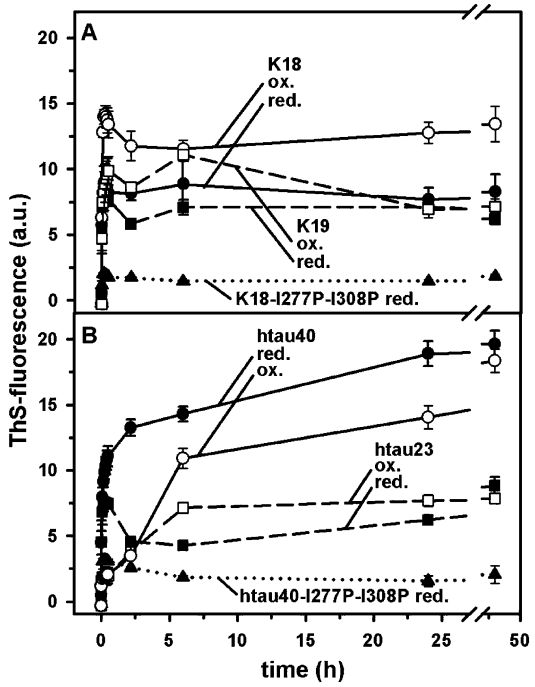

FIGURE 8: Tau aggregation in the presence of arachidonic acid. The kinetics of aggregation of K18 and K19 tau constructs into filaments in the presence of arachidonic acid was measured fluorimetrically using the dye ThS. The first 30 min were measured continuously using the same aliquot, later time points were measured using new aliquots of the polymerization reaction. Tau protein concentrations for filament assembly were 4 μM in each case, arachidonic acid 75 μM in PBS pH 7.4, 1 mM DTT. Shown is the average value (n = 3) with the standard deviation. (A) The four-repeat tau construct K18 (solid lines, circles) and the three-repeat tau construct K19 (dashed lines, squares) both show a fast increase of the fluorescence signal within a few minutes. The signal tends to overshoot by ~10−20% but remains roughly at the maximal level for many hours (up to 48 h). The filled or open symbols refer to reducing or oxidizing conditions (= preincubation for 3 days without DTT, see Methods). As a control, the bottom curve (dotted) represents the mutant K18-I277P-I308P which is not competent for filament formation (*16*) but causes a limited initial fluorescence rise. Other proteins (BSA, RNase) generate only a minimal signal in these conditions (not shown). (B) The tau isoforms htau40 (solid lines) and htau23 (dashed lines) in reducing or oxidizing conditions (filled or open symbols). The reduced proteins show a rapid initial increase in the ThS-signal, similar to (A). In the case of htau40, it continues to increase over a period of 2 days, whereas the curve of htau23 shows an overshoot and then increases very slowly. The oxidized proteins display only a small initial fast phase, then followed by a much slower rising phase (half time a few hours) and a further gradual increase over many hours (only htau40). As a control, the bottom curve (dotted) represents the assembly incompetent mutant htau40-I277P-I308P which shows fast but limited initial fluorescence rise but then remains constant at a low level. Electron microscopy confirms that the initial rapid phase is not due to filament formation, and that the proteins with a low ThS signal form few filaments (e.g., htau23) or none at all (proline mutants).

DISCUSSION

This study was undertaken to explain the origin of seemingly contradictory findings on the pathway of tau's aggregation into PHFs or related structures. The importance of this issue is derived from the fact that tau aggregates are hallmarks of Alzheimer's disease, frontodemporal dementias and other "tauopathies" (*4*, *37*, *38*), and that the clinical progression correlates with the distribution of tau aggregates (*39*, *40*). The major difficulty in analyzing the aggregation process has been that it is exceedingly slow in most buffer conditions (days to weeks), owing to the highly soluble nature of tau protein. This meant that aggregation could be monitored at best by electron microscopy (with its inherent limitations in quantification), but not in solution and in real time, which in turn precluded in-depth kinetic and structural investigations. Major efforts in several laboratories were therefore directed toward increasing the speed of tau aggregation in vitro. This included the choice of recombinant tau-derived constructs (e.g., the repeat domain aggregates faster than full-length tau isoforms (*5*)), oxidation (because disulfide cross-linked dimers accelerate aggregation (*6*)), polyanions (e.g., heparin, acidic peptides, RNA, because they compensate the repulsive positive charges on tau (*8*−*10*)), and certain tau mutations occurring in FTDP-17 (*41*−*43*). In particular, the mutations P301L and ΔK280 enhance tau's propensity for beta-structure and thus facilitate aggregation (*16*, *25*). These improvements have allowed real time observations of aggregation in solution, using appropriate solution assays such as fluorescence or light scattering (*7*, *13*). Other conditions for accelerating tau aggregation were developed by Binder's group (*11*, *12*, *24*): They used free fatty acids as cofactors, e.g., arachidonic acid, and a reducing buffer including DTT, which resulted predominantly in straight fibers rather than PHFs in the strict sense. This raised the question of how the aggregation process described by Binder's group related to that of others, and how the different approaches mirrored tau's aggregation in the diseased neuron (which contains ~90% paired helical and ~10% straight fibers (*20*)). The discrepancy between assembly conditions, i.e., reducing vs oxidizing environment,

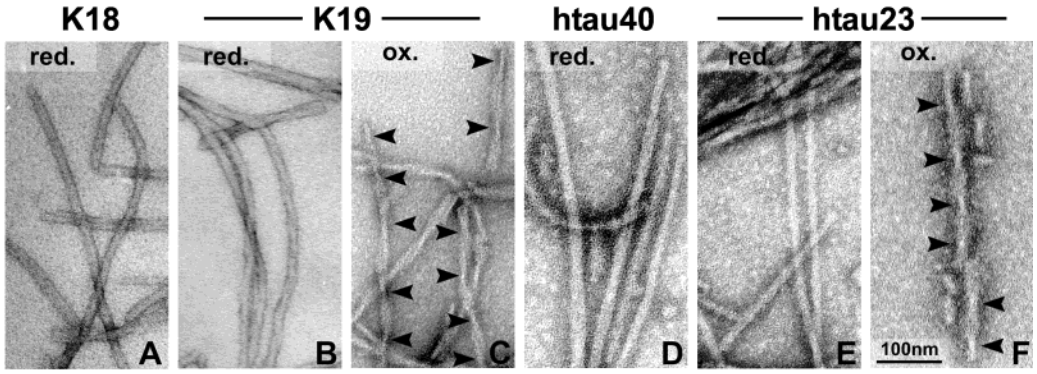

FIGURE 9: Negative stain electron microscopy of tau filaments induced with arachidonic acid. Filaments of tau isoforms or constructs assembled in the presence of arachidonic acid (same filament preparations as for the kinetic data (see Figure 8) at the endpoint of assembly); bar = 100 nm. The four-repeat tau construct K18 and the longest isoform htau40 showed exclusively straight filaments independently of the oxidative state (A, D), although filaments formed under oxidizing conditions were much shorter (not shown). In contrast, the three-repeat tau construct K19 and the shortest isoform htau23 showed a typical paired helical appearance polymerized under oxidative conditions (C, F) and straight filaments under reducing conditions (B, E).

and polyanions vs free fatty acids as cofactors, suggested that the resulting filaments might have a fundamentally different structure and assembly pathway.

On the basis of the results described here, we believe that the different experimental approaches can be explained within a common framework, and that the aggregation products are closely related and representative of abnormal aggregation of tau. First, the effect of fatty acids can be explained by noting that the acceleration of tau aggregation becomes prominent only above the critical micelle concentration (for arachidonic acid ~25 μM (*12*)). Thus, arachidonic acid micelles can be regarded effectively as polyanions because the negatively charged carboxyl groups are exposed on the surface, burying the hydrocarbon chains inside. They would therefore be capable of compensating tau's positive charges similarly to the polyanions we have used, such as heparin. The common features of the aggregates are highlighted by the fact that the repeat domain is important as the backbone of the filaments, both with polyanions (e.g., heparin) and AA micelles. In both cases, the twisted appearance of PHFs is favored by 3R-constructs or isoforms, whereas 4R-forms are less twisted and often smooth and straight (Figures 6 and 9). Thus, while the basic packing of subunits in the fibers seems to be similar, subtle differences can cause variations in the degree of twisting. Examples are the number of repeats (3R or 4R (*9*), and this report), the charge distribution near the repeat boundaries (*44*), or the propensity for beta-structure (since the 4R-mutant K18-ΔK280, which has the highest beta-propensity, forms the most regular twisted filaments (*25*)).

In this context, it is interesting to make a comparison of the inducers of tau aggregation on a molecular basis. A broadly balanced ratio of polyanion to tau is required to achieve rapid assembly, but excess of either partner slows it down again (*14*). This is typical of coacervate-like interactions between charged polymers which are also observed with other microtubule-interacting molecules (*45*). In the case of heparin 6000, optimal assembly was achieved at concentrations around 6 μM in our experimental conditions, with tau protein concentrations in the 25 μM range, yielding a tau/polyanion ratio of roughly 4:1. A similar relationship can be argued in the case of arachidonic acid: For inducing assembly, AA must be above its CMC (~25 μM) and has to obey an optimal ratio with respect to tau (see data of King et al., 1999 (*12*), and Friedhoff et al., 1998 (*14*)). The number of AA molecules in a micelle is variable and not exactly known in our conditions (75 μM AA). Furthermore, the size of the micelles cannot be determined directly (e.g., by negative stain electron microscopy), because lipid micelles cannot be visualized reliably by this method and in any case they would be destroyed by the procedure. But taking a typical diameter of ~10 nm, we estimate ~100 AA molecules per micelle, so that the micelle concentration would be ~1 μM. At 4 μM tau, this yields a ratio of tau/polyanion ~4:1, comparable to the ratio used with heparin. These calculations are highly simplified, but they show that the two assembly systems can be viewed in an analogous fashion. Even the sizes of the polyanions are of comparable magnitude: An average molecule in heparin 6000 contains about 10 disaccharides, and since it is unbranched it has an extended length of ~10 nm, similar to the estimated micelle size of AA. Beyond this formal similarity, it is likely that the different charge distributions on the surface of AA micelles and heparin molecules make a difference to tau aggregation and to the binding of the reporter dye ThS. This may explain the rapid and disproportionate initial increase in fluorescence, observed with AA but not with heparin (see below). Once more it must be stressed that the above considerations are based on rough estimates and are therefore somewhat speculative but they suggest that AA-induced as well as polyanion-induced PHF assembly share similar properties in terms of size and concentrations of the inducing agent. Independently of these considerations, the main point is that both systems of PHF induction can be related to another.

It is less straightforward to explain the seeming discrepancy between oxidative and reductive conditions for tau aggregation. We believe that this can be explained by subtle variations in tau's nucleation and elongation in combination with different polyanions or fatty acids, which highlights different roles of subdomains. In the case of polyanions, the N-terminal domain reduces the assembly competence for 3R- and 4R-isoforms (*10*). By contrast, in the case of AA the N-terminal domain can actually improve polymerizability, provided that the inserts are present, as in htau40. This has been explained by a model where the hairpin folding of the

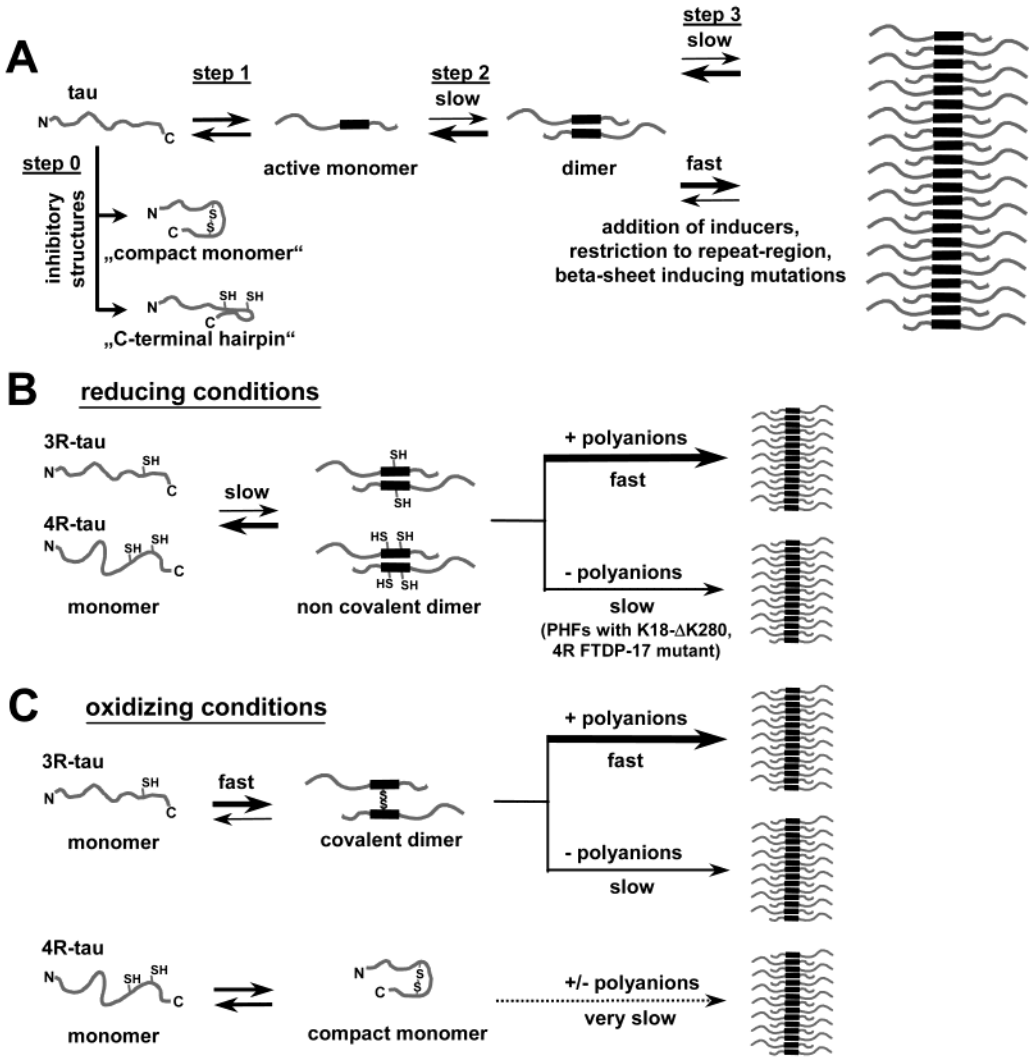

FIGURE 10: Pathways of tau aggregation. (A) Generalized mechanism: step 1, soluble tau normally adopts a mostly random-coil structure (*57*), but can undergo a conformational change where part of the repeat domain adopts an extended conformation (here shown as black bar), ready to enter beta-sheet interactions with other molecules (*15*, *16*). Step 2: Two tau molecules align to form a dimer (presumably by beta-sheet formation around the hexapeptide motifs in R2 or R3). Step 3: Further tau monomers or dimers associate, forming a nucleus and growing into a filament. Step 0: If a tau molecule is locked in the "wrong" conformation (e.g., compact monomer of a four-repeat tau, or tau isoforms without inserts in the presence of arachidonic acid (C-terminal hairpin structure (*12*, *24*, *34*) it cannot promote aggregation, and possibly even inhibits aggregation. For normal soluble tau, k_{-1} and k_{-2} are large so that the equilibrium is shifted to the left; dimers do not form at all or only transiently, and aggregation is negligible. The equilibrium can be shifted to the right toward aggregation by increasing available tau concentrations (e.g., by detachment from microtubules), removal of N- or C-terminal tau domains (because the repeats form the cores for aggregation) or FTDP-17 mutations (facilitating the transition to beta-structure), oxidation (when it leads to stabilized dimers), and polyanions or fatty acid micelles (which improve "stickiness" of tau by charge compensation). (B), (C) Aggregation of 3R-tau and 4R-tau in reducing and oxidizing conditions: In reducing conditions (B), 3R-tau or 4R-tau can undergo the required conformational change and form noncovalent dimers, but polyanions must be present to drive the reaction toward aggregation. An exception to the rule is 4R-tau with the ΔK280 mutation which shows appreciable PHF aggregation even without polyanions because of its high propensity for beta-structure and interactions. In oxidizing conditions (C) in the case of 3R-tau, covalent dimerization at C322 pushes the equilibrium toward aggregation; the reaction is further accelerated by polyanions. In the case of 4R-tau, the intramolecular disulfide bridge locks tau in an inactive conformation which does not aggregate readily, even if polyanions are present. In the case of AA-induced aggregation, the state of oxidation is of secondary importance, but instead an inhibitory state prevails when tau lacks the N-terminal inserts.

C-terminal tail of tau can block aggregation of the repeat domain, but the N-terminal inserts can relieve the blockade, thus facilitating aggregation (*12*, *24*, *34*). In the case of polyanion-induced aggregation, a greater emphasis appears to lie on the folding of the repeat domain. 3R-isoforms can undergo intermolecular cross-linking, favoring dimerization and aggregation. In this case, oxidation accelerates aggregation (*6*, *14*, *31*). With 4R-isoforms the situation is less clear-cut and depends on initial conditions, because oxidation can either accelerate aggregation (if intermolecular disulfide bridges are formed) or inhibit it (if intramolecular disulfide bridges are formed as in the case of the compact cross-linked monomers). In general, with polyanions the requirement for oxidation as an assembly promoting factor is less critical than without polyanions, and even less in the presence of AA micelles. In Alzheimer brain tissue, dimerization could conceivably affect not only tau's aggregation but also its binding to microtubules. However, the binding of tau

monomers and dimers to microtubules is almost indistinguishable (*46*), so that oxidation would matter mainly for tau aggregation.

The above considerations can be summarized by the models of Figure 10. The basic scheme (Figure 10A) starts with a tau monomer which can undergo a conformational change (step 1) which likely entails the formation of extended beta-strands in the repeat domain (*15*) and perhaps deblocking of inhibitory folds such as that of the compact monomer (a hairpin within the repeat domain (*6*)) or a hairpin between the repeats and the C-terminal flanking region (*10*, *12*, *24*, *34*, *47*). This leads to dimers based on the repeat domain (step 2) and hence to polymers whose core consists of repeat domains (step 3). The basic steps are reversible, in principle, but they can become irreversible by covalent modifications, such as disulfide bridges. In particular, the initial dimer is likely to be short-lived and might not last long enough for further subunit addition. It can become long-lived by oxidation, particularly of the single C322 in the three-repeat isoforms, and in this case oxidation speeds up further aggregation. On the other hand, oxidation can also lead to unproductive conformations that are unable to integrate into PHFs. This is the case of the covalent intramolecular cross-link C291−C322 which is possible only with four-repeat tau. These differences between three-repeat and four-repeat tau are illustrated in Figure 10B,C. Similarly, unproductive conformations can be generated if one domain folds over the repeats and renders it unable to interact with others. In this scheme, the fractions of inactive and active tau monomers depend on their domain composition and how they interact with the polyanions or AA micelles, but the reaction pathway is comparable, leading to comparable aggregates.

The analysis of tau aggregation is often confounded with the problem of detectability. Electron microscopy is the only method to judge the nature of the aggregates, but it is of limited use for quantitation. The binding of ThS and concomitant rise in fluorescence is reasonably quantitative for polyanion-induced aggregation. This was shown in an earlier study where the ThS-signal correlated with the amount of pelletable material and no early burst in the ThS-signal occurred (*7*). However, this is not the case with fatty acids such as AA (Figure 8). In the latter case, the dominant and rapid initial increase in ThS fluorescence is not caused by filament assembly as such because filaments are nearly absent at this stage (by electron microscopy) and only develop later and gradually, with comparatively little further change in fluorescence (Figures 8 and 9; see also Figure 3 and Figure 4 in King et al., 1999 (*12*)). Thus, light scattering appears more suitable for measuring AA-induced aggregation (*13*). Nevertheless, the initial increase in ThS fluorescence is indicative of polymerizability. A comparable phenomenon has been observed by studying the binding properties of tau to microtubules. Addition of high amounts of tau leads to an overloading of tau on the microtubules which is accompanied by a rise in the ThS-signal. Electon microscopy of these microtubules showed an unstructured accumulation of tau on the microtubule surface (*48*). These observations are consistent with a model in which nuclei or incipient filaments are formed rapidly, not yet visible by electron microscopy but able to bind and induce ThS fluorescence. The later slow stage of filament formation would take place by annealing of the initial oligomers without major changes in the fluorescence. Thus, in the case of AA the steps of oligomerization and annealing merit further attention, but this would be beyond the present report and is not included in Figure 10.

We have considered above the influence of tau domains, oxidation, or overall folding on tau's rates of self-assembly. Other factors are notable in this context, in particular tau mutations and phosphorylation. Several mutations in the tau gene have been linked to dementia (FTDT-17, for an overview see refs *4* and *38*)). Their mode of action may not be uniform, but some of them appear to enhance aggregation by facilitating the transition to beta-structure within the repeat domain. This holds particularly for the mutations ΔK280 and P301L which are located in or near the beta-forming hexapeptide motifs in repeats 2 and 3 (*16*, *25*). In the scheme of Figure 10, this would enhance step 1 (see Figure 5). Conversely, proline mutants introduced into these motifs disrupt the beta-propensity and thus render the molecule largely incapable of PHF-formation (see Figure 8). The first hexapeptide motif and its ΔK280 mutation are near residue C291, one of the two cysteines whose cross-linking is responsible for the inactive compact monomer. A high beta-propensity could explain why the ΔK280 mutation promotes PHF formation regardless of inhibitory compact monomers (the same argument would apply to P301L). It is interesting to note that the same sequence around the ΔK280 mutation, especially the double lysine motif Lys-280 and Lys-281, is important for the interaction between tau and microtubules (*49*, *50*). In the case of phosphorylation, the relationship to PHF aggregation remains enigmatic. In Alzheimer's disease, tau is both abnormally phosphorylated and aggregated, and certain phospho-epitopes are enriched before the appearance of full-blown tangles (*51*−*54*). However, this does not necessarily imply that phosphorylation of tau promotes its aggregation. On the contrary, in vitro experiments show that phosphorylation protects tau against aggregation (*55*). Thus, the major effect of phosphorylation is indirect, it causes the detachment of tau from microtubules and thereby increases the concentration of unbound tau which could contribute to abnormal aggregation (*56*). In any case, most insights into the mechanism of aggregation were obtained with unphosphorylated tau, and therefore the models of Figure 10 make no assumptions about phosphorylation.

In summary, there are different methods of generating PHFs in vitro which formerly appeared incompatible with each other. However, we argue that they can be traced back to a common set of principles, based on a unified reaction scheme. Differences can be explained by the relative magnitudes of reaction rates and are therefore not considered fundamental. Since the differences are essentially kinetic in nature it is possible to compare them on a relative weighting scale. For example, the natural resistance of tau to aggregate can be overcome either by polyanions (an extrinsic factor), by "correct" oxidation forming a dimer (an extrinsic factor making use of tau's cysteines), or by tau mutations promoting beta-structure (an intrinsic factor). These considerations will be important when assessing factors or drugs designed to suppress the aggregation of tau in neurons, and thus to prevent one of the crucial steps in Alzheimer's disease.

ACKNOWLEDGMENT

We thank Jacek Biernat for providing the tau plasmids, Li Li for providing the proline mutated tau proteins, Mathias Bilang and Karin Blume for excellent technical assistance with protein preparations, and Eva-Maria Mandelkow and Martin von Bergen for insightful suggestions.

REFERENCES

1. Garcia, M. L., and Cleveland, D. W. (2001) *Curr. Opin. Cell. Biol. 13*, 41−8.
2. Goedert, M., Spillantini, M. G., and Davies, S. W. (1998) *Curr. Opin. Neurobiol. 8*, 619−32.
3. Buee, L., Bussiere, T., Buee-Scherrer, V., Delacourte, A., and Hof, P. R. (2000) *Brain Res. Brain Res. Rev. 33*, 95−130.
4. Reed, L. A., Wszolek, Z. K., and Hutton, M. (2001) *Neurobiol. Aging 22*, 89−107.
5. Wille, H., Drewes, G., Biernat, J., Mandelkow, E. M., and Mandelkow, E. (1992) *J. Cell Biol. 118*, 573−584.
6. Schweers, O., Mandelkow, E. M., Biernat, J., and Mandelkow, E. (1995) *Proc. Natl. Acad. Sci. U.S.A. 92*, 8463−7.
7. Friedhoff, P., Schneider, A., Mandelkow, E. M., and Mandelkow, E. (1998) *Biochemistry 37*, 10223−30.
8. Perez, M., Valpuesta, J. M., Medina, M., Montejo de Garcini, E., and Avila, J. (1996) *J. Neurochem. 67*, 1183−90.
9. Goedert, M., Jakes, R., Spillantini, M. G., Hasegawa, M., Smith, M. J., and Crowther, R. A. (1996) *Nature 383*, 550−3.
10. Kampers, T., Friedhoff, P., Biernat, J., and Mandelkow, E. M. (1996) *FEBS Lett. 399*, 344−49.
11. Wilson, D. M., and Binder, L. I. (1997) *Am. J. Pathol. 150*, 2181−95.
12. King, M. E., Ahuja, V., Binder, L. I., and Kuret, J. (1999) *Biochemistry 38*, 14851−9.
13. Gamblin, T. C., King, M. E., Dawson, H., Vitek, M. P., Kuret, J., Berry, R. W., and Binder, L. I. (2000) *Biochemistry 39*, 6136−44.
14. Friedhoff, P., von Bergen, M., Mandelkow, E. M., Davies, P., and Mandelkow, E. (1998) *Proc. Natl. Acad. Sci. U.S.A. 95*, 15712−17.
15. von Bergen, M., Friedhoff, P., Biernat, J., Heberle, J., Mandelkow, E. M., and Mandelkow, E. (2000) *Proc. Natl. Acad. Sci. U.S.A. 97*, 5129−34.
16. von Bergen, M., Barghorn, S., Li, L., Marx, A., Biernat, J., Mandelkow, E. M., and Mandelkow, E. (2001) *J. Biol. Chem. 276*, 48165−74.
17. Giannetti, A. M., Lindwall, G., Chau, M. F., Radeke, M. J., Feinstein, S. C., and Kohlstaedt, L. A. (2000) *Protein Sci. 9*, 2427−35.
18. Wischik, C. M., Novak, M., Thogersen, H. C., Edwards, P. C., Runswick, M. J., Jakes, R., Walker, J. E., Milstein, C., Roth, M., and Klug, A. (1988) *Proc. Natl. Acad. Sci. U.S.A. 85*, 4506−10.
19. Novak, M., Kabat, J., and Wischik, C. M. (1993) *EMBO J. 12*, 365−370.
20. Crowther, R. A. (1991) *Proc. Natl. Acad. Sci. U.S.A. 88*, 2288−92.
21. Biernat, J., Mandelkow, E. M., Schröter, C., Lichtenberg-Kraag, B., Steiner, B., Berling, B., Meyer, H. E., Mercken, M., Vandermeeren, A., Goedert, M., and Mandelkow, E. (1992) *EMBO J. 11*, 1593−7.
22. Goedert, M., Wischik, C., Crowther, R., Walker, J., and Klug, A. (1988) *Proc. Natl. Acad. Sci. U.S.A. 85*, 4051−4055.
23. Gustke, N., Trinczek, B., Biernat, J., Mandelkow, E. M., and Mandelkow, E. (1994) *Biochemistry 33*, 9511−22.
24. King, M. E., Gamblin, T. C., Kuret, J., and Binder, L. I. (2000) *J Neurochem. 74*, 1749−57.
25. Barghorn, S., Zheng-Fischhofer, Q., Ackmann, M., Biernat, J., von Bergen, M., and Mandelkow, E. (2000) *Biochemistry 39*, 11714−11721.
26. Schagger, H., Cramer, W. A., and von Jagow, G. (1994) *Anal. Biochem. 217*, 220−30.
27. Heukeshoven, J., and Dernick, R. (1988) *Electrophoresis 9*, 28−32.
28. Cleveland, D. W., Hwo, S. Y., and Kirschner, M. W. (1977) *J. Mol. Biol. 116*, 227−47.
29. Lee, G., Cowan, N., and Kirschner, M. (1988) *Science 239*, 285−8.
30. Rizzu, P., Van Swieten, J. C., Joosse, M., Hasegawa, M., Stevens, M., Tibben, A., Niermeijer, M. F., Hillebrand, M., Ravid, R., Oostra, B. A., Goedert, M., van Duijn, C. M., and Heutink, P. (1999) *Am. J. Hum. Genet. 64*, 414−21.
31. Bhattacharya, K., Rank, K. B., Evans, D. B., and Sharma, S. K. (2001) *Biochem. Biophys. Res. Commun. 285*, 20−6.
32. Ksiezak-Reding, H., and Yen, S. H. (1991) *Neuron 6*, 717−28.
33. Goedert, M., Spillantini, G., Cairns, N. J., and Crowther, R. A. (1992) *Neuron 8*, 159−168.
34. Carmel, G., Mager, E. M., Binder, L. I., and Kuret, J. (1996) *J. Biol. Chem. 271*, 32789−95.
35. Abraha, A., Ghoshal, N., Gamblin, T. C., Cryns, V., Berry, R. W., Kuret, J., and Binder, L. I. (2000) *J. Cell Sci. 113 Pt 21*, 3737−45.
36. Pollanen, M. S., and Bergeron, C. (2000) *Acta Neuropathol. (Berl) 99*, 534−8.
37. Spillantini, M. G., and Goedert, M. (1998) *Trends Neurosci. 21*, 428−33.
38. Buee, L., and Delacourte, A. (1999) *Brain Pathol. 9*, 681−93.
39. Braak, H., and Braak, E. (1991) *Acta Neuropath. 82*, 239−59.
40. Arriagada, P. V., Growdon, J. H., Hedley-Whyte, E., and Hyman, B. T. (1992) *Neurology 42*, 631−639.
41. Hutton, M., Lendon, C. L., Rizzu, P., Baker, M., Froelich, S., Houlden, H., Pickering-Brown, S., Chakraverty, S., Isaacs, A., Grover, A., Hackett, J., Adamson, J., Lincoln, S., Dickson, D., Davies, P., Petersen, R. C., Stevens, M., de Graaff, E., Wauters, E., van Baren, J., Hillebrand, M., Joosse, M., Kwon, J. M., Nowotny, P., Heutink, P., and et al. (1998) *Nature 393*, 702−5.
42. Spillantini, M. G., Murrell, J. R., Goedert, M., Farlow, M. R., Klug, A., and Ghetti, B. (1998) *Proc. Natl. Acad. Sci. U.S.A. 95*, 7737−41.
43. Poorkaj, P., Bird, T. D., Wijsman, E., Nemens, E., Garruto, R. M., Anderson, L., Andreadis, A., Wiederholt, W. C., Raskind, M., and Schellenberg, G. D. (1998) *Ann. Neurol. 43*, 815−25.
44. DeTure, M. A., Di Noto, L., and Purich, D. L. (2002) *J. Biol. Chem. 277*, 34755−9.
45. Erickson, H. P., and Voter, W. A. (1976) *Proc. Natl. Acad. Sci. U.S.A. 73*, 2813−7.
46. Di Noto, L., DeTure, M. A., and Purich, D. L. (1999) *Mol. Cell Biol. Res. Commun. 2*, 71−6.
47. Lichtenberg-Kraag, B., Mandelkow, E. M., Biernat, J., Steiner, B., Schroter, C., Gustke, N., Meyer, H. E., and Mandelkow, E. (1992) *Proc. Natl. Acad. Sci. U.S.A. 89*, 5384−8.
48. Ackmann, M., Wiech, H., and Mandelkow, E. (2000) *J. Biol. Chem. 275*, 30335−43.
49. Goode, B. L., and Feinstein, S. C. (1994) *J. Cell Biol. 124*, 769−82.
50. Goode, B. L., Chau, M., Denis, P. E., and Feinstein, S. C. (2000) *J. Biol. Chem. 275*, 38182−9.
51. Braak, E., Braak, H., and Mandelkow, E. M. (1994) *Acta Neuropathol. 87*, 554−67.
52. Bancher, C., Brunner, C., Lassmann, H., Budka, H., Jellinger, K., Wiche, G., Seitelberger, F., Grundke-Iqbal, I., Iqbal, K., and Wisniewski, H. M. (1989) *Brain Res. 477*, 90−9.
53. Jicha, G. A., Lane, E., Vincent, I., Otvos, L., Jr., Hoffmann, R., and Davies, P. (1997) *J. Neurochem. 69*, 2087−95.
54. Augustinack, J. C., Schneider, A., Mandelkow, E. M., and Hyman, B. T. (2002) *Acta Neuropathol. (Berl) 103*, 26−35.
55. Schneider, A., Biernat, J., von Bergen, M., Mandelkow, E., and Mandelkow, E. M. (1999) *Biochemistry 38*, 3549−58.
56. Yoshida, H., and Ihara, Y. (1993) *J. Neurochem. 61*, 1183−6.
57. Schweers, O., Schonbrunn-Hanebeck, E., Marx, A., and Mandelkow, E. (1994) *J. Biol. Chem. 269*, 24290−7.

BI026469J